Jour. of Radiosurgery and SBRT, Vol. 5, pp. 171-181
Reprints available directly from the publisher
Photocopying permitted by license only

Clinical Investigation

Assessment of concurrent stereotactic radiosurgery and bevacizumab treatment of recurrent malignant gliomas using multi-modality MRI imaging and radiomics analysis

Chunhao Wang, Wenzheng Sun, John Kirkpatrick, Zheng Chang and Fang-Fang Yin

Department of Radiation Oncology, Duke University, Durham, NC 27710, USA

Correspondence to: Fang-Fang Yin, PhD, Department of Radiation Oncology, Duke University Medical Center, Durham, NC 27710, USA; Email: fangfang.yin@duke.edu; Phone: +1 (919) 660-2180; Fax: +1 (919) 681-7183

(Received: January 26, 2018; Accepted: March 16, 2018)

ABSTRACT

Purpose: To assess the response and predict the overall survival (OS) of recurrent malignant gliomas (MG) patients treated with concurrent BVZ/SRS using multi-modality MRI imaging and radiomics analysis.

Methods and materials: SRS was delivered in a single fraction (18/24Gy) or 25Gy in 5 fractions. BVZ was administered immediately before SRS and 2 weeks after. MRI scans were performed before SRS, 1 week and 2 months after SRS. The MR protocol included 2 anatomical (T1w and T2w) and 2 functional (dynamic contrast-enhanced DCE-MRI and diffusion weighted DW-MRI) modalities. Functional biomarkers including apparent diffusion coefficient (ADC), micro-vascular transfer constant Ktrans, brain blood flow F_B, and blood volume V_B were analyzed. Radiomics analysis was performed to extract imaging features from anatomical MRI images and functional biomarker maps. Wicoxon signed rank tests were performed to evaluate treatment-induced changes, and Mann-Whitney U tests were performed to compare the differences of treatment-induced changes between different patient groups. Selected biomarkers and radiomics features were used to predict the OS after treatment using Support Vector Regression (SVR) with leave-one-out cross validation (LOOCV).

Results: Twelve patients with recurrent MG were studied. The median OS was 13.8 months post SRS. DCE results showed that Ktrans (p=0.035) and V_B (p=0.035) showed significant decrease 2 months after SRS, and F_B showed significant decrease as early as 1 week (p=0.017) after SRS. No functional parameters reflected statistically significant treatment response 1 week after SRS. A total of 888 radiomics features were extracted. 31/126 features demonstrated significant changes 1 week/2 months after SRS, respectively. 9 features' changes were significantly different between WHO Grade III vs IV patient groups, and 6 features' changes were found to be linearly correlated with OS. Using 5 selected features, 9 patients' survival time could be accurately predicted (Mean absolute error = 1.47 months, RMSE = 2.10 months).

Conclusion: The results of this work demonstrate the potential of combined radiomics analysis and functional MR imaging in quantitatively identifying early treatment response of concurrent SRS/BVZ.

Keywords: DCE-MRI, DW-MRI, SRS, recurrent glioma, radiomics, treatment assessment

INTRODUCTION

Malignant gliomas are the most common primary malignant brain tumors in the United States, and 80% of them are glioblastoma (GBM). Virtually all glioblastoma patients treated with the current standard of care (maximum safe surgical resection followed by concurrent radiotherapy and temozolomide) will recur, with a <5% 5-year progression-free survival rate [1,2]. Treatment of recurrent malignant gliomas is challenging. Combining stereotactic radiosurgery (SRS) with an antiangiogenic agent bevacizumab BVZ (Genetech, San Francisco, CA) for the treatment of recurrent malignant gliomas is conceptually appealing. SRS has demonstrated reasonable long survival of recurrent malignant gliomas [3]. However, ionizing radiation could upregulate vascular endothelial growth factor, leading to angiogenesis stimulation [4]; on the other hand, BVZ could counteract radiation-induced angiogenesis as a reduction of tumor growth support. In addition, BVZ could mitigate radiation-induced inflammation, edema, and necrosis associated with hypofractionated radiotherapy [5]. However, BVZ is not a benign entity, as severe side effects, including thromboembolic phenomena, malignant hypertension, and visceral perforation have been reported occasionally [6]. Thus, the combined SRS/BVZ regimen requires prudent assessment of treatment effect and potential outcome correlation studies to demonstrate its safety and efficacy.

MR functional quantitative imaging offers an approach to extract functional information from MR images. MR functional quantitative imaging has a distinguished feature of estimating functional information in a joint session with anatomical imaging session while maintaining the desired high spatial resolution of anatomical MR images. In addition, the zero ionizing radiation risk makes MR functional quantitative imaging a good candidate for longitudinal *in vivo* studies with repeated acquisitions over a short period [7]. Of the available functional modalities, diffusion-weighted MRI (DW-MRI) and dynamic contrast enhanced MRI (DCE-MRI) are among the most frequently employed ones for radiotherapy treatment assessment and outcome prediction [8,9,10,11]. DW-MRI utilizes the sensitivity of MR to Brownian motion of water molecules. With different strengths of diffusion weighting in the sequence coding, apparent diffusion coefficient (ADC) as a logarithmic parameter of MR signal decay can be derived as an indicator of tissue cellular density [12]. DCE-MRI acquires series of T1w MR images before, during and after the intravenous injection of a low molecular, T1-shortening paramagnetic contrast agent (CA). The evaluation of CA can be estimated as a linear function of T1 value change. Vascular functions, including blood flow, perfusion volume and microvessel permeability can be quantitatively calculated using compartmental pharmacokinetic (PK) models [13]. The imaging biomarkers from DW-MRI and DCE-MRI could provide quantitative assessment of cell killing and angiogenesis of this concurrent SRS/BVZ regime.

Another potential tool for treatment assessment is the emerging field of radiomics. Radiomics refers to the automated extraction of mineable data from standard-of-care medical images with great throughput potentials [14]. The quantitative signatures after computational image processing may serve as non-invasive measurements of tissue phenotypes, including histopathology, biochemical variations, and genetic mutation [15]. Because of the superior soft tissue contrast in anatomical MRI and rich physiological information in functional MRI, MR-based radiomics analysis has been demonstrated in preliminary studies as an attractive tool of clinical decision making for therapeutic outcome assessment [16,17,18].

This study critically determines the performance of functional MR imaging as well as radiomics analysis in monitoring treatment response of the concurrent SRS/BVZ regime. Specifically, we hypothesize that: 1) functional imaging can reflect noticeable changes during the longitudinal imaging course; and 2) radiomics features can serve as indicators of treatment response. There are two points that distinguish this study from other similar works: 1) Multiple MRI studies, including one pre-treatment and two post-treatment scans, improved our ability to accurately assess treatment response; and 2) radiomics study results and functional imaging findings were jointly investigated for possible OS prediction

METHODS AND MATERIALS

Patients

In this IRB approved retrospective study, twelve adult patients with WHO grade III or IV recurrent malignant glioma were included. Patient selection criteria include the initial enrollment requirement [19], availability of OS and completed imaging studies (1 pre-treatment and 2 post-treatment scans). Following standard treatment with surgery followed by radiation therapy and concurrent adjuvant temozolomide, all patients completed concurrent SRS/BVZ treatment.

Treatment

In this SRS/BVZ regime, BVZ was administered intravenously (10 mg/kg) about 24 hours before the start

of SRS as the first dose. A second BVZ dose (10mg/kg) was given to the patients about 2 weeks after the first dose. Table1 summarizes some key patient demographics and key statistics of treatment.

For SRS treatment, patients were immobilized with a U-frame thermoplastic facemask (BrainLAB, Munich, Germany). Gross tumor volume (GTV) was defined as the contrast-enhancing lesion on post-contrast T1w MR volume, and PTV was generated as a 1mm uniform expansion of GTV. PTVs <2 cm and 2-2.9 cm in greatest dimension were prescribed with 24 Gy or 18 Gy in a single fraction, respectively, and PTVs with 3-5 cm greatest dimension were prescribed with 25 Gy total in 5 consecutive daily fractions. The SRS delivery methods included dynamic conformal arc (DCA) and Volumetric Modulated Arc Treatment (VMAT) techniques (Table1). All SRS fractions were delievered on a Novalis Tx system (Varian and BrainLAB) with a robotic 6D couch. Imaging protocol prior to each delivery included orthogonal kilovolt imaging (2D-3D match) and cone beam CT imaging (3D-3D match). Patient positions were corrected in a 6D fashion (translations, couch rotation, pitch and roll) after 2D-3D and 3D-3D matches.

MR imaging

All patients received 3 MRI exams using a bird-cage quadrature head coil on a 1.5T MR scanner (General Electric, Fairfield CT) in our department. The pre-treatment MRI exam was performed about 24 hours before 1st BVZ administration and was treated as 'baseline' scan. Two post-treatment MRI exams were performed 1 week and 2 months after SRS, respectively.

In each exam, DW-MRI scans were performed after anatomical T1w and T2w scans. DW-MRI scans were acquired axially using a spin-echo echo planar imaging (EPI) sequence: TR = 9,100ms, TE = 98ms, field of view (FOV) = 300x300mm^2, matrix size = 256x128, slice thickness = 5mm, gap = 0mm, no average. Two sets of images were acquired with different diffusion weighting factors *b=500s/mm2* and *b=0.* The ADC map was calculated as a logarithmic parameter of the MR signal ratio using 2 different *b*-value volumes [20].

DCE-MRI scans were performed using a 3D spoiled-gradient recalled-echo (SPGR) sequence: TR = 6.2ms, TE = 2.0ms, flip angle = 15°, FOV = 300x210mm^2, matrix size 256x128, slice thickness = 2.5mm. Prior to the dynamic scan, the 3D SPGR sequences were acquired at variable flip angles of 5°, 10°, 15°, 20°, and 30° to calculate the pre-contrast tissue T1 value (T_{10}) [21]. Then, the CA gadolinium-diethylenetriamine pentaacetic acid (Magnevist) was administered with a dose of 0.2mmol/kg body and a flow rate of 3mL/s, followed by a bolus injection of 20mL saline. The dynamic scan was performed in a partial portion of brain containing the PTV at a temporal resolution of 5.25s, and a series of 3D volumes at 32-40 post-injection time points were recorded.

At each post-injection time point, the tissue T1 map ($T_1(t)$) were calculated using the dual flip angle method (5° and 15°) with the general assumption TE<T_2^* [22]. The CA concentration *C(t)* in each voxel was calculated as a linear dependence of tissue longitudinal relaxation rate (1/T1) change:

Table 1. Patient demographics and key statistics
AO = anaplastic oliodendoglioma; GBM = glioblastoma; AA = anaplastic astrocytoma;
KPS = Karnofsky performance score; DCA = dynamic conformal arc ; VMAT = volumetric modulated arc therapy

No.	Gender	Histology	WHO grade	Initial KPS	SRS technique	SRS Rx	OS (mo)
1	M	AO	III	100%	DynArc	1800 cGy x 1	29.4
2	M	GBM	IV	100%	VMAT	500 cGy x 5	18.5
3	M	GBM	IV	80%	DynArc	1800 cGy x 1	16
4	M	AA	III	80%	DynArc	2400 cGy x 1	5.3
5	M	AO	III	90%	DynArc	2400 cGy x 1	26.2
6	F	GBM	IV	100%	DynArc	2400 cGy x 1	19.5
7	M	AO	III	90%	VMAT	500 cGy x 5	5.9
8	M	AA	III	90%	DynArc	1800 cGy x 1	5.8
9	M	GBM	IV	90%	DynArc	1800 cGy x 1	6.2
10	F	AA	III	80%	VMAT	1800 cGy x 1	11.5
11	M	GBM	IV	100%	DynArc	1800 cGy x 1	18.3
12	F	GBM	IV	90%	VMAT	500 cGy x 5	8.8

$$rC(t) = 1/T_1(t) + 1/T_{10} \quad (1)$$

where r is the longitudinal relaxivity of the CA ($4.3 mM^{-1}s^{-1}$ at 1.5T magnetic field) [23]. Three quantiative biomarkers from two commonly used DCE-MRI PK models were investigated in this study. First, the classic extended Tofts model was analyzed to quantify K^{trans}, which models the permeability rate of CA exchange between blood plasma and extravascular extracellular space (EES) [24]. K^{trans} has served as the primary quantitative functional biomarker in many oncologic DCE-MRI studies [25]. The CA dynamics in blood plamsa, referred as arterial input function AIF, was approximated using an experiment-based polulation averaging AIF model [26].

The two-compartment exchange model was adopted to quantify the brain blood flow F_B and blood volume V_B [27]:

$$C(t) = F_B \int_0^t AIF(u).[e^{-K_+(t-u)} + E(e^{-K_-(t-u)} - e^{-K_+(t-u)})]du \quad (2)$$

where were related to the reciprocal CA exchange rate constants between blood plasma and EES, and E is a parameter associated with and circulation transit time ($=V_B/F_B$). Fitting Eq.(2) with measured $C(t)$ and prior AIF knowledge by Levenberg-Marquardt algorithm with zero initial conditions, the blood volume V_B can be estimated from F_B as:

$$F_B / V_B = K_+ - E(K_+ - K_-) \quad (3)$$

Both post-treatment scans were registered to the pre-treatment scan. For each functional MR biomarker (ADC, K^{trans}, F_B, V_B), the volumetric mean value in 4 region-of-interest (ROIs) were recorded: GTV, PTV, V12Gy (toxicity indicator [28]) and V12Gy-PTV (normal tissue). To examine the functional change captured after treatment, Wilcoxon signed rank tests were performed for each post-treatment scans in comparison with the baseline data. Mann-Whitney U tests were performed to evaluate the possible difference of parameters' normalized changes between WHO grade III and IV patient groups, where the normalized change Δ was defined as the ratio of post-treatment value to pre-treatment value (Δ = value[post 1/2 scan]/ value[baseline]) . Spearman's rank correlation coefficients (r) were calculated between OS and the normalized change of each biomarker.

Radiomics analysis

An in-house radiomics analysis software was used to analysis 6 MR volume series, including 4 function maps (ADC, K^{trans}, F_B, V_B) as well as anatomical T1w and T2w images. In each MR volume, radiomics features were analyzed within 4 ROIs (GTV, PTV, V12Gy and V12Gy–PTV). In each ROI, 43 unique quantitative features in 4 categories (Figure 1) that collectively capture MR texture signature were extracted:

1) Intensity features: describe the shape characteristics of the MR volume's gray-level intensity histogram, i.e., a probability density function (PDF) of gray-level distribution
2) Morphological features: describe the morphological characteristics of the ROI [29].
3) Coarse texture features: describe the low-resolution heterogeneity in the ROI. These features were calculated from the ROI's Gray-Level Run Length Matrix (GLRLM), a joint PDF that measures the size of a set of consecutive voxels with the same grayscale intensity at a given direction [30].
4) Fine texture features: describe the high-resolution heterogeneity in the ROI. These features were derived from the ROI's Gray-Level Co-Occurrence Matrix (GLCOM), a joint PDF that measures the frequency of co-occurring adjacent voxel pairs having the same grayscale intensity at a given direction [31].

Radiomics analysis was performed for all three MR exams. Wilcoxon signed rank tests were performed to determine the change of each radiomics feature value after treatment, and the statistical significance level was set to 0.05 with Bonferroni correction [32]. Mann-Whitney U tests were performed to compare the differences of feature change between WHO grade III and IV patient groups. Spearman's rank correlation coefficients (r) were calculated between OS and the normalized change of each radiomics feature.

OS prediction

To explore the potential joint use of functional MR biomarkers and radiomics features for OS prediction, selected features with high coefficient r values in correlation tests were investigated with support vector regression (SVR) to predict OS with leave-one-out cross validation (LOOCV) [33].

RESULTS

Functional MR analysis

Figure 2 shows the comparison of functional MR parametric maps from a selected patient (No. 11 in Table 1) on all three MR exam days. The DCE-MRI biomarker maps (K^{trans}, F_B and V_B) demonstrated elevated intensity distribution around PTV region in the pre-treatment scan. This observation confirmed microvessel abnormality of the PTV region. In the 1st post-treatment scan, these 3 maps showed minor changes; in contrast, the decrease of intensity in all three maps could be easily appreciated in 2nd post-treatment scan, suggesting a suppression of microvessel activity. The ADC distribution from DW-MRI did not demonstrate noticeable differences in Figure 2.

Figure 3 summarizes all patients' normalized changes of functional MR biomarkers in 1st and 2nd post treatment scans. The DCE-MRI functional biomarkers in (a)-(c) appeared to be trending lower following SRS, especially in PTV and GTV. The normalized changes in the 1st post-treatment scan were heterogeneous within the patient cohort; in contrast, the normalized changes in the 2nd post-treatment scan converged towards low values, indicating a substantial decrease in functional microvessel activity as treatment response after two months. The ADC value did not reveal noticeable changes along the imaging study course.

Table 2 lists the statistics of functional MR parameters. Compared to the pre-treatment scan baseline values, in the 2nd post-treatment scan, mean values of K^{trans} and V_B in PTV, GTV and V12Gy were significantly lower. Note that the decreases of blood flow F_B in PTV and GTV were significant in both post-treatment scans,

Intensity

#	Short	Feature Name
1	I -1	Energy
2	I -2	Entropy
3	I -3	Skewness
4	I -4	Kurtosis

Morphological

#	Short	Feature Name
5	M-1	Volume
6	M-2	Surface Area
7	M-3	Sphericity
8	M-4	Spherical Disproportion
9	M-5	Compactness 1
10	M-6	Compactness 2

Coarse Texture

#	Short	Feature Name
11	C-1	Short Run Emphasis
12	C-2	Long Run Emphasis
13	C-3	Gray Level Non-Uniformity
14	C-4	Run Length Non-Uniformity
15	C-5	Run Percentage
16	C-6	Low Gray Level Run Emphasis
17	C-7	High Gray Level Run Emphasis
18	C-8	Short Run Low Gray Level Emphasis
19	C-9	Short Run High Gray Level Emphasis
20	C-10	Long Run Low Gray Level Emphasis
21	C-11	Long Run High Gray Level Emphasis

Fine Texture

#	Short	Feature Name
22	F-1	Autocorrelation
23	F-2	Cluster Prominence
24	F-3	Cluster Shade
25	F-4	Cluster Tendency
26	F-5	Contrast
27	F-6	Correlation
28	F-7	Difference Entropy
29	F-8	Dissimilarity
30	F-9	GLCOM Energy
31	F-10	GLCOM Entropy
32	F-11	Homogeneity 1
33	F-12	Homogeneity 2
34	F-13	Informational Measure of Correlation 1
35	F-14	Informational Measure of Correlation 2
36	F-15	Inverse Difference Moment Normalized
37	F-16	Inverse Difference Normalized
38	F-17	Inverse Variance
39	F-18	Maximum Probability
40	F-19	Sum Average
41	F-20	Sum Entropy
42	F-21	Sum Variance
43	F-22	Variance

Figure 1. Radiomics features in 4 categories

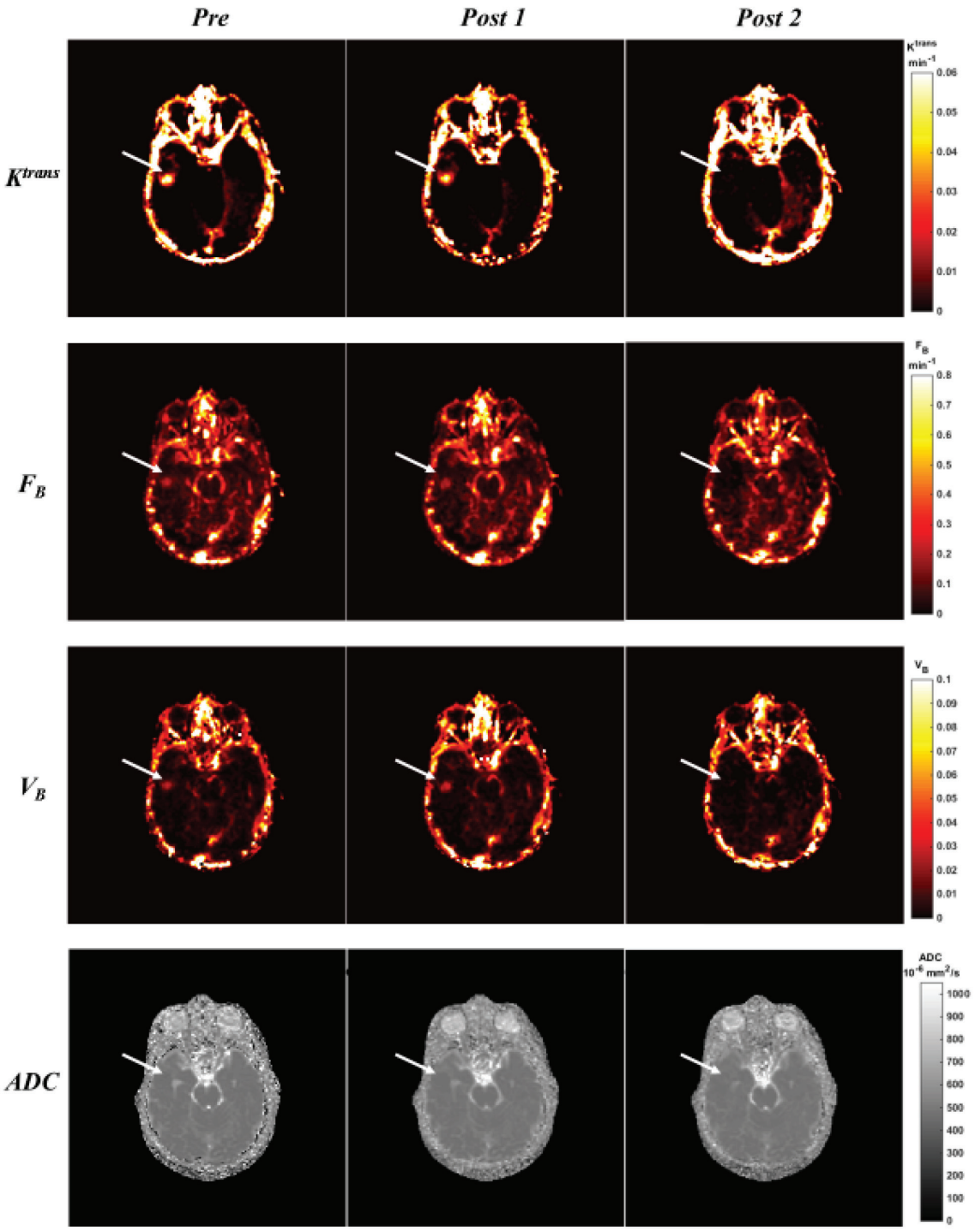

Figure 2. A comparison of functional MR parametric maps from a selected patient. White arrows indicate the PTV location

earlier than the other two DCE-MRI biomarkers. No biomarkers showed difference between WHO grade III and IV patients. Although the decrease of F_B in PTV was found to be linearly correlated with patient OS ($|r|$=0.82), this correlation was not significant

Radiomics analysis

Figure 4 presents the normalized changes (in logarithmic scale) of the analyzed radiomics features in both post-treatment scans. Since the same ROIs derived

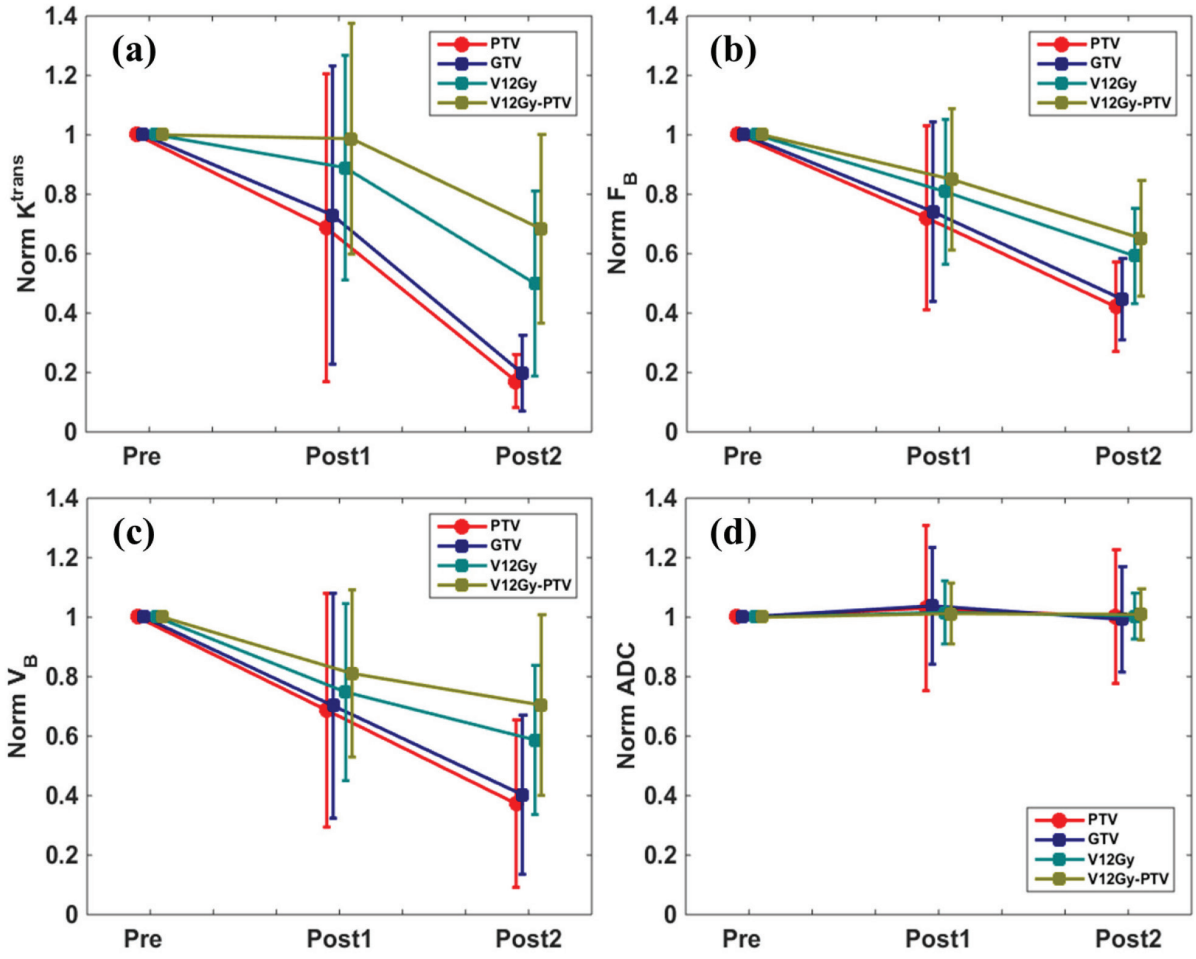

Figure 3. Normalized changes (Post[1/2] value/Pre value) of functional MR parameters. The dots represent the group mean value and the error bars represent the sample variation.

from the pre-treatment scans were used for the registered post-treatment scans, the morphological features (M-1 to M-6 in Figure 1) were excluded. The normalized changes of radiomics features were heterogeneous among different features, and certain features demonstrated extreme normalized change up to 60 in the 2nd post-treatment scans.

Of 888 investigated radiomics features, 126 features (14.2 %) had significant changes in the 2nd post-treatment scan. In these 126 features, 102 features were found in PTV or GTV. Interestingly, the other 24 features in V12Gy and V12Gy-PTV were all found in anatomical T1w or T2w scans (T1w: 13 in V12Gy, 5 in V12Gy-PTV; T2w: 2 in V12Gy, 4 in V12Gy-PTV), and none of the radiomics features from functional MR biomarker maps in V12Gy or V12Gy-PTV had significant changes. In the 1st post-treatment scan, 31 features (3.5%) demonstrated statistically significant changes. Among these 31 features, 28 of them came from anatomical scans, 1 came from F_B (C-11 in GTV), and 2 came from ADC (C-8 in V12Gy and V12Gy-PTV). Note that none of the ADC radiomics features showed significant changes in the 2nd post-treatment scan. The following features from anatomical images demonstrated significant changes in both post-treatment scans:

T1w: F-5, F-11, F-12, F-15, F-16 , C-1, C-2, C-4, C-5 in both GTV and PTV
T2w:F-13 in both GTV and PTV; F-13, C-2 and C11 in V12Gy-PTV

None of the radiomics features from functional MR biomarker maps changed significantly in both post-treatment scans.

In the 1st post-treatment scan, normalized changes of 7 features in V12Gy-PTV from T2w scan (I-2, F-14, F-17, F-20, C-1, C-2, C-5) demonstrated significant differences between WHO grade III and IV patient groups; in contrast, only two features from DCE-MRI biomarker maps (K^{trans}: C-6 in PTV; F_B: C-8 in PTV)

Table 2. Summary of functional parameter statistics. * indicates statistically significant change

Para	ROI	*Pre scan*	*Post 1 scan*	*Post 2 scan*
K^{trans}	*PTV*	0.0183 ± 0.0115	0.0104 ± 0.0084	0.0030 ± 0.0054* (*p=0.035*)
min^{-1}	*GTV*	0.0196 ± 0.0155	0.0147 ± 0.0195	0.0064 ± 0.0033* (*p=0.035*)
	V12Gy – PTV	0.0100 ± 0.0068	0.0080 ± 0.0065	0.0058 ± 0.0091* (*p=0.035*)
		0.0084 ± 0.0055	0.0075 ± 0.0073	0.0065 ± 0.0080
F_B	PTV	0.0992 ± 0.0721	0.0687 ± 0.0581* (*p=0.017*)	0.0368 ± 0.0214* (*p=0.017*)
min^{-1}	GTV	0.0921 ± 0.0622	0.0680 ± 0.0565* (*p=0.017*)	0.0392 ± 0.0247* (*p=0.035*)
	V12Gy	0.0800 ± 0.0441	0.0682 ± 0.0481	0.0498 ± 0.0349
	V12Gy – PTV	0.0766 ± 0.0399	0.0685 ± 0.0456	0.0530 ± 0.0388
V_B	*PTV*	0.0127 ± 0.0093	0.0069 ± 0.0067	0.0034 ± 0.0022* (*p=0.017*)
	GTV	0.0117 ± 0.0087	0.0066 ± 0.0061	0.0037 ± 0.0028* (*p=0.035*)
	V12Gy – PTV	0.0100 ± 0.0072	0.0066 ± 0.0047	0.0056 ± 0.0052* (*p=0.035*)
		0.0095 ± 0.0070	0.0067 ± 0.0044	0.0062 ± 0.0060
ADC	*PTV*	2664.4 ± 579.1	2704.8 ± 870.3	2609.3 ± 543.7
10^{-6}	*GTV*	2664.8 ± 514.8	2755.4 ± 752.5	2621.6 ± 558.0
mm^2/s	*V12Gy – PTV*	2749.1 ± 517.1	2794.4 ± 623.6	2744.1 ± 477.2
		2766.3 ± 550.0	2792.5 ± 603.4	2765.7 ± 463.0

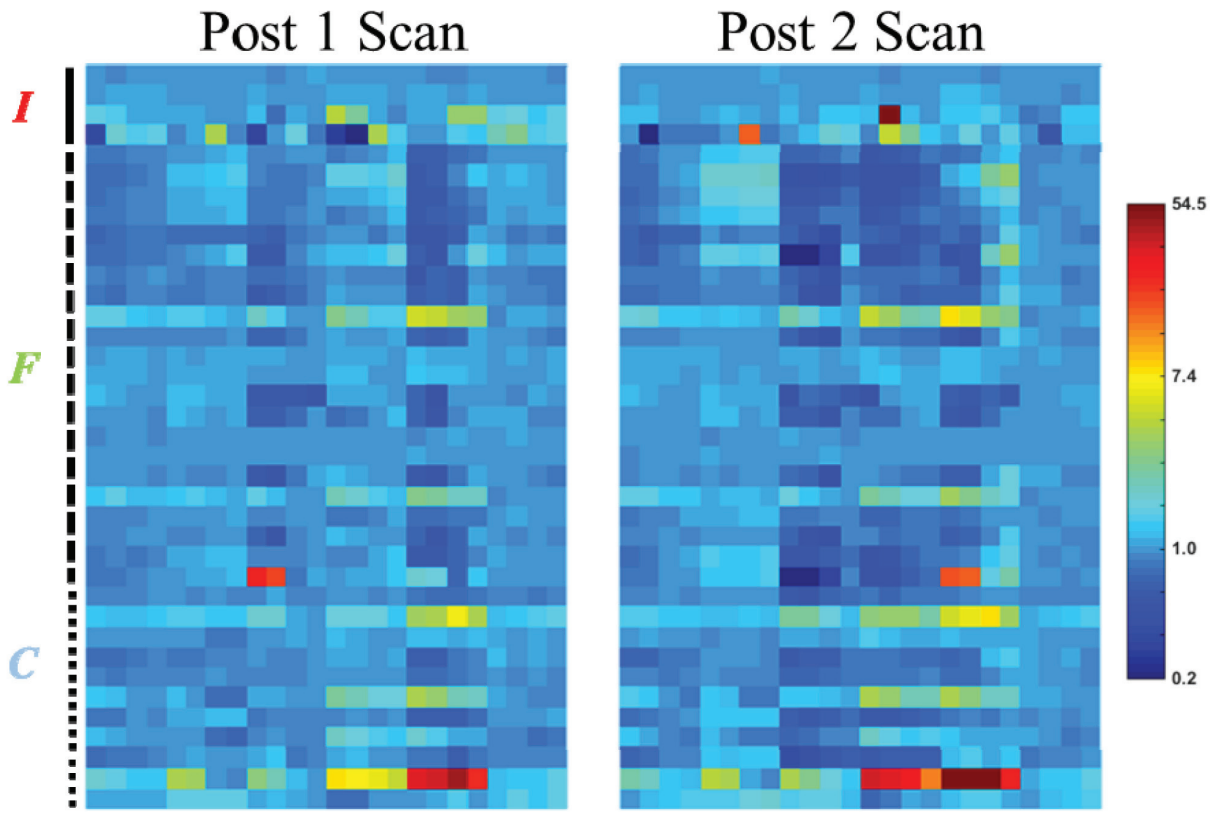

Figure 4. Normalized changes (Post[1/2] value/Pre value) of radiomics features in different ROIs in both post-treatment scans. The normalized changes are color-coded in logarithmic scale.

Each voxel represents an extracted feature (I: intensity feature; F: fine texture feature; C: coarse texture feature)

demonstrated significant differences between the two groups. Regarding the relationship between radiomics feature change and OS, 4 PTV features from T1w images in the 1st post-treatment scan (F-2, F-3, C-9, C-10) and 2 PTV features in the 2nd post-treatment scan (F_B: C-1; ADC: C-7) were found to be linearly correlated with OS.

OS prediction

When using a selected group of 5 features' normalized changes (K^{trans}: C-6 in PTV; *ADC*: C-7 in PTV; T1w: F-2 and C-7 in PTV; C-7 in GTV) in the 2nd post-treatment scan for outcome prediction, 9 out of 12 patients' OS time were accurately predicted (Mean absolute error = 1.47 mo, RMSE = 2.10 mo).

DISCUSSION

In this work, the therapeutic response of the combined BVZ/SRS regime was assessed by multiple post-treatment MR exams. The functional biomarkers from DCE-MRI captured the microvessel functional change in the PK parametric maps. The BVZ selectively binds to and neutralizes the functional activity of vascular endothelial growth factor (VEGF) [34]. Such neutralization can lead to impaired tumor vascularization, which may be reflected by the decrease of perfusion/permeability rate in DCE-MRI [35]. The longitudinal study in this work showed that the commonly used DCE-MRI biomarker K^{trans} changed significantly in the 2nd post-treatment scan, but not in the earlier 1st post-treatment scan. This observation was consistent with a similar animal study that involved BVZ and DCE-MRI [36]. Based on this finding, for a better clinical utility, post-treatment functional imaging should be performed a few weeks after, not immediately after the combined SRS/BVZ treatment, to capture greater K^{trans} change. In comparison, the F_B captured significant changes in PTV as early as in the 1st post-treatment scan with only 1 BVZ dose, suggesting that F_B could be more sensitive to the BVZ effect than K^{trans}. When intra-course evaluation imaging available, F_B could serve as early indicator for treatment response for possible adaptive therapy.

Unlike DCE-MRI, the ADC from DW-MRI did not exhibit significant changes during the treatment course. ADC is dominated by the fraction of intracellular water; thus, tissue with decreased cell density (decreased intracellular water fraction) would lead to an increased ADC measurement [37]. The ADC results in Figure 3 may suggest that progressive cell killing was not observed, possibly due to repopulation immediately following SRS. Of note, 2 radiomics features from ADC maps (C-8 in V12Gy and V12Gy-PTV) demonstrated significant changes only in the 1st post-treatment scan. Mathematically, C-8 was defined to emphasize the heterogeneity at low intensity regions [30]. The decrease of C-8 may suggest the dispersed response to radiation damage in normal tissue (V12Gy-PTV), with possibly elevated ADC intensity as cell killing evidence. In the 2nd post-treatment scan (two months after SRS), such dispersion was undermined by the normal tissue recovery.

The radiomics analysis of functional MR biomarker maps found out more indicators of therapeutic response in addition to the conventional biomarker statistics. Some feature changes were found to be correlated with OS, suggesting the potential use of radiomics features for prognosis beyond standard image analysis. Most features in DCE-MRI biomarker maps with significant changes were found in PTV or GTV, possibly because the microvessel activity in the disease area with abnormal functional behavior. One of the key findings in this work is that radiomics features from anatomical T1w and T2w scans demonstrated potential values in capturing therapeutic response. In the 1st post-treatment scan, 28 features from T1w and T2w scans showed significant changes in comparison with baseline results. This strongly supports the argument that radiomics analysis could reveal the hidden information in image texture that may reflect potential physiological change in the medical images [18, 38]. The difference of T1w and T2w feature change between different WHO grades patients may provide guidelines of desired early treatment response, which could be further investigated for early treatment intervention. In the 2nd post-treatment scan, the features with significant changes were found in large volumes containing normal tissue (V12Gy and V12Gy - PTV). This fact suggests that anatomical MR images could be used to assess normal tissue response to the concurrent BVZ/SRS, which would be difficult to achieve within functional MR biomarker maps.

One of the limitation in the current work is the limited patient number. To provide better clinical guidelines of functional imaging utilization , retrospective/perspective studies with larger cohort sizes are in demand. In addition, larger patient cohort sizes allow more complicated statistical analysis and machine learning techniques for improved prognosis value. Another limitation is the sole OS information as treatment outcome. In this work, only a small portion of patient had completed biochemistry lab results and genetic evaluations. Because of limited samples, such information could not be incorporated in the statistical analysis and prediction modelling. It would be of great clinical interests if radi-

omics features could be correlated with these outcomes in future studies with larger cohort sizes.

CONCLUSIONS

The quantitative functional MR imaging and multi-modality MR radiomics analysis described in this study provided insight into the response of recurrent malignant gliomas treated with concurrent SRS/BVZ. Certain functional MR biomarkers and radiomics features appear to capture the early therapeutic response. Joint utilization of features from functional/anatomical MR images may aid in predicting patient OS. Future studies with larger cohort sizes is in demand to provide better clinical guidelines.

ACKNOWLEDGMENTS

Authors' disclosure of potential conflicts of interest
This research did not receive any specific grant from funding agencies in the public, commercial, or not-for-profit sectors.
Dr. John Kirkpatrick reports grants from Genentech, grants from Varian Medical Systems, other from ClearSight RT Products; Dr. Fang-Fang Yin received research grants from NIH and Varian Medical Systems. Also, as invited speakers for Varian Medical Systems and Brainlab.

Author contributions
Conception and design: Fang-Fang Yin, John Kirkpatrick, Zheng Chang
Data collection: Chunhao Wang, Fang-Fang Yin, Zheng Chang
Data analysis and interpretation: Chunhao Wang, Wenzheng Sun, Fang-Fang Yin
Manuscript writing: Chunhao Wang, Wenzheng Sun
Final approval of manuscript: Chunhao Wang, Wenzheng Sun, John Kirkpatrick, Zheng Chang, Fang- Fang Yin

REFERENCES

1. Ostrom QT, et al. CBTRUS statistical report: Primary brain and central nervous system tumors diagnosed in the United States in 2008-2012. Neuro-oncology 2015;17:iv1-iv62.
2. Stupp R, et al. Effects of radiotherapy with concomitant and adjuvant temozolomide versus radiotherapy alone on survival in glioblastoma in a randomised phase iii study: 5-year analysis of the EORTC-NCIC trial. Lancet Oncology 2009;10:459-466.
3. Fogh SE, et al. Hypofractionated stereotactic radiation therapy: An effective therapy for recurrent high-grade gliomas. Journal of Clinical Oncology 2010;28:3048-3053.
4. Moeller BJ, et al. Pleiotropic effects of hif-1 blockade on tumor radiosensitivity. Cancer Cell 2005;8:99-110.
5. Levin VA, et al. Randomized double-blind placebo-controlled trial of bevacizumab therapy for radiation necrosis of the central nervous system. International Journal of Radiation Oncology Biology Physics 2011;79:1487-1495.
6. Armstrong TS, et al. Management of treatment-associated toxicites of anti-angiogenic therapy in patients with brain tumors. Neuro-oncology 2012;14:1203-1214.
7. Chang Z Wang C. Treatment assessment of radiotherapy using mr functional quantitative imaging. World Journal of Radiology 2015;7:1.
8. Kim CK, Park BK, Lee HM. Prediction of locally recurrent prostate cancer after radiation therapy: Incremental value of 3t diffusion-weighted MRI. Journal of Magnetic Resonance Imaging 2009;29:391-397.
9. King AD, et al. DCE-MRI for pre-treatment prediction and post-treatment assessment of treatment response in sites of squamous cell carcinoma in the head and neck. PloS One 2015;10:e0144770.
10. Lambrecht M, et al. Value of diffusion-weighted magnetic resonance imaging for prediction and early assessment of response to neoadjuvant radiochemotherapy in rectal cancer: Preliminary results. International Journal of Radiation Oncology Biology Physics 2012;82:863-870.
11. Wang C, et al. Assessment of treatment response with diffusion-weighted MRI and dynamic contrast-enhanced MRI in patients with early-stage breast cancer treated with single-dose preoperative radiotherapy: Initial results. Technology in Cancer Research and Treatment 2016;15:651-660.
12. Kauppinen RA. Monitoring cytotoxic tumour treatment response by diffusion magnetic resonance imaging and proton spectroscopy. NMR in Biomedicine 2002;15:6-17.
13. O'Connor JP, et al. DCE-MRI biomarkers in the clinical evaluation of antiangiogenic and vascular disrupting agents. British Journal of Cancer 2007;96:189-195.
14. Kumar V, et al. Radiomics: The process and the challenges. Magnetic Resonance Imaging 2012;30:1234-1248.
15. Aerts HJ, et al. Decoding tumour phenotype by noninvasive imaging using a quantitative radiomics approach. Nature Communications 2014;5.
16. Alic L, et al. Heterogeneity in DCE-MRI parametric maps: A biomarker for treatment response? Physics in Medicine and Biology 2011;56:1601.
17. Parmar C, et al. Radiomic feature clusters and prognostic signatures specific for lung and head and neck cancer. Scientific Reports 2015;5:11044.
18. Vallières M, et al. A radiomics model from joint FDG-PET and MRI texture features for the prediction of lung metastases in soft-tissue sarcomas of the extremities. Physics in Medicine and Biology 2015;60:5471.
19. Cabrera, Alvin R., et al. Concurrent stereotactic radiosurgery and bevacizumab in recurrent malignant gliomas: a prospective

trial. International Journal of Radiation Oncology Biology Physics 2013;86.5: 873-879.

20. Le Bihan D, et al. MR imaging of intravoxel incoherent motions: Application to diffusion and perfusion in neurologic disorders. Radiology 1986;161:401-407.

21. Cheng HLM. t1 Measurement of flowing blood and arterial input function determination for quantitative 3d t1-weighted DCE-MRI. Journal of Magnetic Resonance Imaging 2007;25:1073-1078.

22. Schabel MC Morrell GR. Uncertainty in t1 mapping using the variable flip angle method with two flip angles. Physics in Medicine and Biology 2008;54:N1.

23. Tofts PS, et al. Estimating kinetic parameters from dynamic contrast-enhanced t 1-weighted MRI of a diffusable tracer: Standardized quantities and symbols. Journal of Magnetic Resonance Imaging 1999;10:223-232.

24. Sourbron SP Buckley DL. On the scope and interpretation of the tofts models for DCE-MRI. Magnetic Resonance in Medicine 2011;66:735-745.

25. Hylton N. Dynamic contrast-enhanced magnetic resonance imaging as an imaging biomarker. Journal of Clinical Oncology 2006;24:3293-3298.

26. Parker GJ, et al. Experimentally-derived functional form for a population-averaged high-temporal-resolution arterial input function for dynamic contrast-enhanced MRI. Magnetic Resonance in Medicine 2006;56:993-1000.

27. Sourbron S, et al. Quantification of cerebral blood flow, cerebral blood volume, and blood–brain-barrier leakage with DCE-MRI. Magnetic Resonance in Medicine 2009;62:205-217.

28. Lawrence YR, et al. Radiation dose–volume effects in the brain. International Journal of Radiation Oncology Biology Physics 2010;76:S20-S27.

29. Guo W, et al. Prediction of clinical phenotypes in invasive breast carcinomas from the integration of radiomics and genomics data. Journal of Medical Imaging 2015;2:041007-041007.

30. Tang X. Texture information in run-length matrices. IEEE Transactions on Image Processing 1998;7:1602-1609.

31. Haralick RM Shanmugam K. Textural features for image classification. IEEE Transactions on Systems, Man, and Cybernetics 1973;3:610-621.

32. Chen W, et al. Volumetric texture analysis of breast lesions on contrast-enhanced magnetic resonance images. Magnetic Resonance in Medicine 2007;58:562-571.

33. Gu B, et al. Incremental learning for ν-support vector regression. Neural Networks 2015;67:140-150.

34. Jain RK, et al. Lessons from phase III clinical trials on anti-VEGF therapy for cancer. Nature Clinical Practice Oncology 2006;3:24-40.

35. Cohen MH, et al. FDA drug approval summary: Bevacizumab (avastin®) plus carboplatin and paclitaxel as first-line treatment of advanced/metastatic recurrent nonsquamous non-small cell lung cancer. Oncologist 2007;12:713-718.

36. Wang C, et al. Evaluation of the effect of transcytolemmal water exchange analysis for therapeutic response assessment using DCE-MRI: A comparison study. Physics in Medicine and Biology 2016;61:4763.

37. Paran Y, et al. Water diffusion in the different microenvironments of breast cancer. NMR in Biomedicine 2004;17:170-180.

38. Prasanna P, et al. Radiomic features from the peritumoral brain parenchyma on treatment-naive multi-parametric mr imaging predict long versus short-term survival in glioblastoma multiforme: Preliminary findings. European Radiology 2016:1-10.